AHEAD 2020 Scientific/Technical Report - WP 9.8

Understanding the interaction between soft protons and X-ray mirrors

Final report

Reference Period: 02/03/2020 – 01/09/2022

V. Fioretti[1], T. Mineo[2], R. Amato[2], S. Lotti[3], C. Macculi[3], S. Molendi[4], F. Gastaldello[4], G. Lanzuisi[1], M. Cappi[1], M. Dadina[1], S. Ettori[1]

[1]INAF OAS Bologna, [2]INAF IASF Palermo, [3]INAF IAPS Roma, [4]INAF IASF Milano

Project acronym:
AHEAD2020

Project Title:
Integrated Activities for the High Energy Astrophysics Domain

Grant Agreement No: **871158**
**This deliverable is part of a project that has received funding from the European Union's
Horizon 2020 research and innovation programme**

Start date of the project:
2020-03-02

Version	Revision Date	Review/Approval
1.0	1/09/2022	Creation date
1.1	3/10/2022	Internal review
1.2	14/10/2022	Included comments by WP leaders

Distribution List	Date	Version
AHEAD2020 WP 9	5/10/2022	1.1
AHEAD2020 WP 9	14/10/2022	1.2

0. Explanation of the work carried out within the WP

Low energy (< 300 keV) protons entering the field of view of the XMM-Newton telescope and scattering with the mirror surface are observed in the form of a sudden increase in the background level. Such flaring events, affecting about 30-40% of the XMM-Newton observing time, can hardly be disentangled from true X-ray events and cannot be rejected on board. All future high throughput gracing incidence X-ray telescopes operating outside the radiation belts (e.g. ATHENA) are potentially affected by soft proton induced contamination that must be foreseen and limited since the design phase. On the other side, a clear description of the interaction model would link the observed soft proton spectra by XMM-Newton to the ones hitting the telescope pupil, mapping the low energy particle environment along its orbit.

Thanks to the latest validation studies on the physics models describing the reflection process of protons at grazing angles, we build a proton response matrix for the XMM-Newton and ATHENA missions, describing the effective area and energy redistribution of protons entering the mirror aperture. The simulation pipeline comprises two independent simulation frameworks for the X-ray optics reflectivity, based on ray-tracing and Geant4, and a Geant4 simulation for the proton transmission efficiency caused by the combination of optical filters, on-chip electrodes and the detection depletion regions, requiring a detailed mass model of the focal plane assemblies.

The response matrix for protons will allow a better understanding of the proton radiation environment, with the aim of modeling the in-flight non X-ray background of current and future X-ray focusing telescopes. The XMM-Newton matrix will be used to analyze the mean energy spectra of the background flares, converting the mission into a "proton telescope", while characterizing its particle background. The matrices for the ATHENA telescope will allow for a fast evaluation of the soft proton induced background for any input population, driving the design of shielding solutions.

The response matrix is formatted according to the NASA OGIP (Office of Guest Investigators Program) calibration database (caldb) format, and it consists of an RMF and ARF file in FITS (Flexible Image Transport System) format. X-ray data analysis tools available to the X-ray astronomy community such as *Xspec* and *SPEX* can be used to simulate or analyse the soft proton-induced background spectra.

0.1 Activity breakdown

The following table shows the breakdown of the present WP, with the activity structured in three subWPs, two dedicated to the production of the proton response matrix for the XMM-Newton and ATHENA use cases, and the last dedicated to data formatting, verification and validation.

	subWPs	Tasks	1YEAR			2YEAR			
			Q1	Q2	Q3	Q1	Q2	Q3	Q1 + 2 months
1	XMM-Newton soft proton response matrix	1.1 EPIC soft proton spectra extraction (IASF-Mi)							
		1.2 Geant4 XMM soft proton scattering (OAS)							
		1.3 Ray-tracing XMM soft proton scattering (IASF-Pa)							
		1.4 Geant4 proton attenuation simulation (IAPS)							
2	ATHENA soft proton response matrix	2.1 Geant4 ATHENA soft proton scattering (OAS)							
		2.2 Ray-tracing ATHENA soft proton scattering (IASF-Pa)							
		2.3 Geant4 X-IFU proton attenuation simulation (IAPS)							
		2.4 Geant4 WFI proton attenuation simulation (OAS)							
3	Data formatting, verification and validation	3.1 Simulation input formatting (OAS)							
		3.2 XMM-Newton and ATHENA proton response matrix (OAS, IASF-Pa, IAPS)							
		3.3 Verification: XMM-Newton and ATHENA proton analysis and comparison with input model (OAS)							
		3.4 Validation: XMM-Newton proton analysis and comparison with environment models (OAS and IASF-Mi)							

(Right margin: "End of project")

Table 1: WP breakdown.

Participants and tasks:
- INAF/OAS:
  - V. Fioretti, G. Lanzuisi, M. Dadina, M. Cappi, S. Ettori
  - Tasks:
    - Management (V. Fioretti)
    - 1.2 (V. Fioretti)
    - 2.1 (V. Fioretti)
    - 2.4 (V. Fioretti)
    - 3.1 (V. Fioretti, G. Lanzuisi)
    - 3.2 (V. Fioretti, G. Lanzuisi)
    - 3.3 (M. Dadina, M. Cappi, S. Ettori)
    - 3.4 (M. Dadina, M. Cappi, S. Ettori)

- INAF/IASF-Mi:
  - S. Molendi, F. Gastaldello
  - Tasks:
    - 1.1 (S. Molendi, F. Gastaldello)
    - 3.2 (S. Molendi, F. Gastaldello)
    - 3.4 (S. Molendi, F. Gastaldello)

- INAF/IASF-Pa:
  - T. Mineo, R. Amato
  - Tasks:
    - 1.3 (T. Mineo, R. Amato)
    - 1.4 (T. Mineo, R. Amato)
    - 2.2 (T. Mineo, R. Amato)

- ■ 3.2 (T. Mineo, R. Amato)

- ● INAF/IAPS:
    - ○ S. Lotti, C. Macculi
    - ○ Tasks:
        - ■ 1.4 (S. Lotti, C. Macculi)
        - ■ 2.3 (S. Lotti, C. Macculi)
        - ■ 3.2 (S. Lotti, C. Macculi)

1. XMM-Newton proton response matrix design (Task 1)

The ESA XMM-Newton X-ray mission was launched in December 1999. In more than 20 years, and counting, of operations has provided a unique observation window to the X-ray Universe at energies below 10 – 15 keV. Orbiting in high eccentricity elliptical orbit, with an apogee > 105 km, XMM-Newton carries three Wolter type-I mirrors to focus X-rays by means of grazing angle reflection with European Photon Imaging Cameras (EPIC) placed at each focal plane.

The XMM-Newton EPIC instrument is the telescope X-ray imager and spectrometer, covering the 0.2 -15 keV energy range. It consists of three cameras: two MOS [1] and one PN CCD [2]. In addition to the focal plane instrumentation, two of the three telescopes are equipped with Reflection Grating Spectrometers (RGS [3]). About 50% of the proton flux is expected for the XMM-Newton EPIC/MOS [4] which is partially shaded by the RGS.

Each X-ray mirror module consists of 58 Wolter type-I coaxial and co-focal Gold-coated Nichel shells [5] composed by a paraboloid and hyperboloid section, with a thickness ranging from 0.47 mm at the inner shell, with a diameter of about 30 cm, to 1.07 mm at the outer 70 cm diameter. The coating thickness is 0.2 μm and the focal length is 7.5 m. An X-ray baffle is placed at the entrance for stray-light suppression in the field of view of the instruments. Its inclusion is mandatory in the mirror simulation because it also reduces the incoming proton flux. The baffle is made of Invar, a Nickel-Iron alloy commonly used for space applications because of its low coefficient of thermal expansion, and it consists of two planes of 59 circular strips and 16 radial spokes at about 10 cm from the mirror entrance.

During observation, the XMM-Newton filter wheel can set the optical blocking filters as:

- thin filter, with 0.16 μm of poly-imide and 0.04 μm of aluminum;

- medium filter, with 0.16 μm of poly-imide and 0.08 μm of aluminum;

- thick filter, with 0.33 μm of polypropylene, and 0.11 μm of aluminum, and 0.045 μm of tin.

Protons lose some of their energy crossing the optical filters, and each of their configuration is associated to a different set of RMF and ARF files.

1.1 EPIC soft proton spectra extraction (Task 1.1)

The EXTraS (Exploring the X-ray Transient and variable Sky) project [6] funded by the FP7 European program, provided an unbiased database of XMM-Newton EPIC blank sky observations collected from 2000 to 2012. This unprecedented collection of data was used in the ESA AREMBES[1] project to characterize both the unfocused and focused observed particle background. Soft proton flares are extremely unpredictable in duration, lasting from 100 s to hours, and intensity. In the intense flares the unfocused background can be assumed negligible and both PN and MOS observations can be analysed using the proton response matrix. If instead we want to extract a representative count rate from the 12 year data-set to compare the best-fit model with the predicted proton environment, the observations must be cleaned not only of source contamination, CXB and instrument noise, but also the level of the unfocused particle background must be kept under control. Since only the MOS detector provides an out-of-FoV region to

---

[1] https://space-env.esa.int/athena-radiation-environment-models-and-x-ray-background-effects-simulators-arembes/

measure the unfocused background component and because of the loss of the MOS1 CCD, only EPIC MOS2 observations were used for this study.

The focused background count rate was extracted with the following conditions:

- only single and double events and standard flags to avoid bright columns and pixels;
- 7 < E < 12 keV to avoid CXB contamination;
- exclusion of the 9.4-10 and 11-12 energy bands to eliminate the Gold fluorescence line;
- only exposures in the Full Window mode to obtain a uniform data-set.

The product of this analysis was a FITS file containing for each 500 sec time bin the count rate of both the in-FoV and out-of-FoV observations, for a total of 106.42 Ms of exposure [7]. The in-FoV minus out-of-FoV count rate cumulative distribution function (CDF) is normalized here in units of counts cm^{-2} s^{-1} keV^{-1}, using the area coverage for the in-FoV observations of 31.2 cm^2 and the selected energy ranges in the data filtering process. The CDF is shown in Fig. 1, from which we can compute the fraction of time spent by the XMM-Newton telescope below a given count rate. The maximum focused background count rate expected in 90% of the observing time is 0.0164 counts cm^{-2} s^{-1} keV^{-1}. In the verification and validation process of Sect. 3 we test the proton response matrix with two different input models of the soft proton environment linked to the magnetosheath regime of the Earth's magnetosphere and the interplanetary solar wind. Since these models refer to the maximum flux expected in 90% of observation time, the simulated background at MOS is compared to the observed CDF 90% count rate, to test the accuracy of the response files but also explore the origin of XMM soft proton flares.

Spectral analysis of in-flight soft proton flares deconvolved with the proton response matrix is also an important validation and study tool. We exploited 13 spectra extracted in [7] from the 12 years data-set for each optical filter combination, on the basis of the discrepancy between the in-FoV and out-of-FoV regions and the intensity of the in-FoV region. We selected the spectrum with a ratio between the in-FoV and out-of-FoV counts between 10 and 20, where we can neglect the unfocused background contamination. The spectrum was then normalized for the CDF 90% rate to obtain a representative intensity. We assume that any dependence of the spectral distribution on the intensity is much lower than the general uncertainties of the present study. The normalised spectrum, obtained from about 200 ks of data, is plotted in Fig. 2.
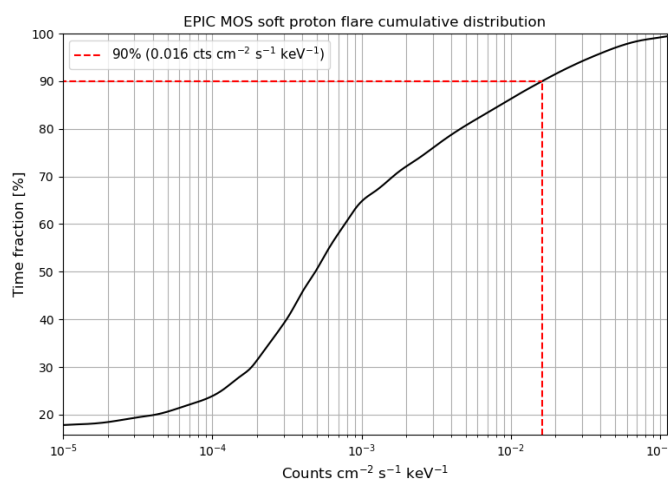

Figure 1: CDF of the EPIC MOS2 focused background count rate. The dashed lines refer to the maximum rate expected in 90% of exposure time.
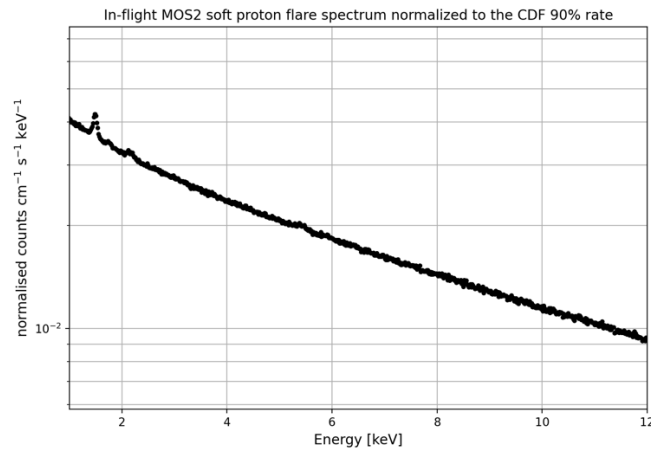
Figure 2: MOS2 X-ray spectrum (medium filter) of high state soft proton flares covering about 200ks of observation, normalised to the CDF 90% count rate.

1.2 Geant4 XMM soft proton scattering (Task 1.2)

The Geant4 toolkit [8, 9] is an open-source particle transport code for Monte Carlo simulations. It allows building 3D models of the instruments, tracking the particle history and storing the results of its interaction. The Geant4-based BoGEMMS framework [10] was used for the Geant4 simulations obtained throughout the work.

The Geant4 mass model of a single XMM-Newton mirror module is shown in Fig. 3 (left), with in grey the X-ray baffle, dark red the Nickel shells and yellow the Gold coating visible in the inner regions. The Wolter-I design is approximated with four cone trunks, intersecting the paraboloid and hyperboloid actual geometry. Fig. 3 (right) shows the simulated spatial distribution of the protons at the mirror exit, for an input mono-energetic beam.

The ability to reproduce the proton scattering interaction with the mirror surface is a key ingredient in the simulation of soft proton induced background. Measurements of proton scattering at grazing angles ($< 1 - 2$ degrees) on the surface of samples of the ATHENA Silicon Pore Optics and eROSITA X-ray mirror [11] and the comparison with Geant4 simulations [12], have defined the driving physics model for the reflection of protons at grazing incident angles. The new detailed validation of Geant4 physics scattering models together with a comprehensive estimate of the systematic uncertainties introduced by the experiments, proved the Coulomb scattering to reproduce experimental observations with sufficient accuracy.

Since the AREMBES and EXACRAD [13] projects provided an extensive validation of the Geant4 10.4 release, we used the same Geant4 version to produce the proton response files, selecting the Single Scattering reference physics list as the electromagnetic physics models of choice, since the Coulomb scattering modelled by the Single Scattering physics list was able to reproduce the eRosita and ATHENA SPO scattering measurement within 1σ [14].

The angular, spatial and intensity distribution of the protons at a given height from the XMM-Newton optical filter were compared to ray-tracing simulations (Sect. 1.3). Since the only impacting difference is in the proton flux intensity because of the different models implementing the proton grazing scattering, we chose the Geant4 mirror simulation as the driver for the proton response matrix production.

A set of mono-energetic runs at each input energy is produced. The proton position, energy, and angular momenta are recorded as a list of events at two heights: 754 mm, the focal plane baffle entrance, and 111 mm, at the optical filter. The comparison of the final count rate between the two cases allows estimating the impact of secondary scattering at the baffle in the focused background flux.
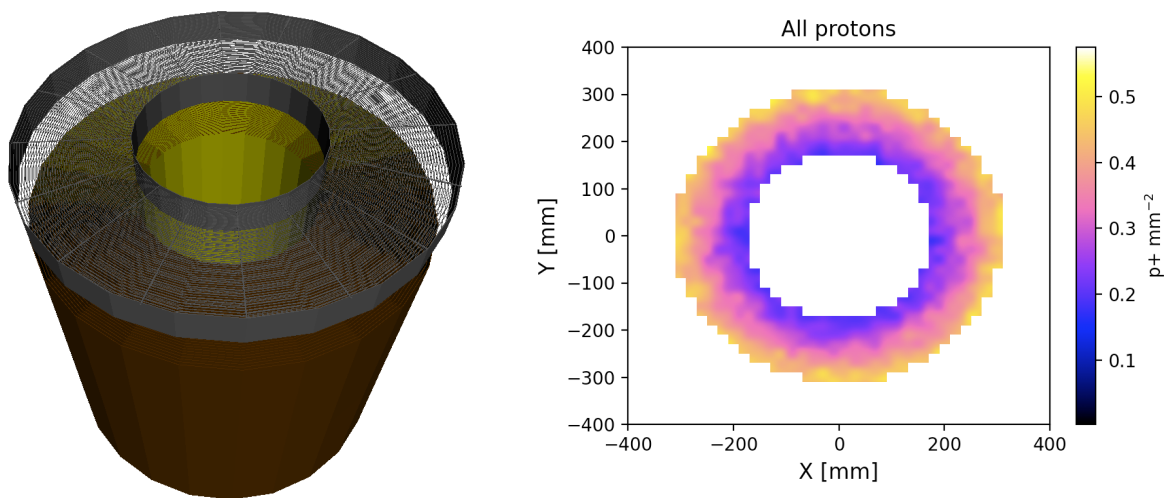

Figure 3: (left) Geant4 mass model of the XMM-Newton mirror module including the X-ray baffle placed at the telescope pupil. (right) Geant4 simulation of the proton spatial distribution at the mirror exit.

1.3 Ray-tracing XMM soft proton scattering (Task 1.3)

The ray-tracing code is a stand-alone software that includes the XMM-Newton optics geometry, the optics baffle and the forward proton shield in front of the detectors. It is able to handle either photon and protons. It follows the particle from the pupil through its interactions with the mirror shells down to the focal plane. At each interaction, it uses a Monte Carlo method to assign the particle angular and energy distribution according to a defined probability model. The photon reflectivity is modelled according to tabulated values [15, 16] and the mirror micro-roughness is taken into account modifying the output specular direction with a Gaussian. The optics geometry has been verified comparing the ray-tracing values of the X-ray on-axis effective area and vignetting at 1.5 keV and 6.4 keV with the nominal ones[2]. Discrepancies between the two sets of curves are always lower than 5%. Two proton reflection models are implemented in the XMM-Newton mirror simulation code:

- the Remizovich model in elastic approximation that assumes a reflection efficiency of 100% and no energy degradation. The output angular distribution is drawn from the Remizovich formulas [17].
- a modified version of the Remizovich model in non-elastic approximation, based on laboratory measurements on eROSITA mirror samples that include the energy lost in the interactions [18]. In

---

[2] Effective area curve from http://xmm.esac.esa.int/external/xmm_user_support/documentation/technical/Mirrors/index.shtml
Vignetting curves from https://xmm-tools.cosmos.esa.int/external/xmm_user_support/documentation/uhb/effareaoffaxis.html

this model the dimensionless parameter σ of the Remizovich solution, that summarizes the physics of the proton interaction with matter, is directly determined by fitting experimental data.

The elastic solution was used in a first version of the XMM-Newton proton response matrix [19] that tested the feasibility of the method. Both implementations were tested in the XMM ray-tracing simulation, but since the final proton distribution is only slightly affected, we chose to use the elastic solution since it considerably decreases the simulation time.

If the same elastic Remizovich model is implemented in the ray-tracing and Geant4 simulation of proton scattering at the XMM mirror, we find a discrepancy of about 15% in scattering efficiency likely caused by the geometrical approximation of the Wolter-I in the Geant4 simulation. If instead the Single Scattering is used in the Geant4 simulation, the scattering efficiency, i.e. the number of protons reaching the focal plane, decreases of a factor 2. Using an input energy of 50 keV at the mirror entrance, we computed and compared the angular and radial distribution of the protons at the top of the optical filters obtained with the Remizovich ray-tracing and the Single Scattering Geant4 simulation, after normalising for the different efficiency. The two distributions, as shown in Fig. 4, are comparable.
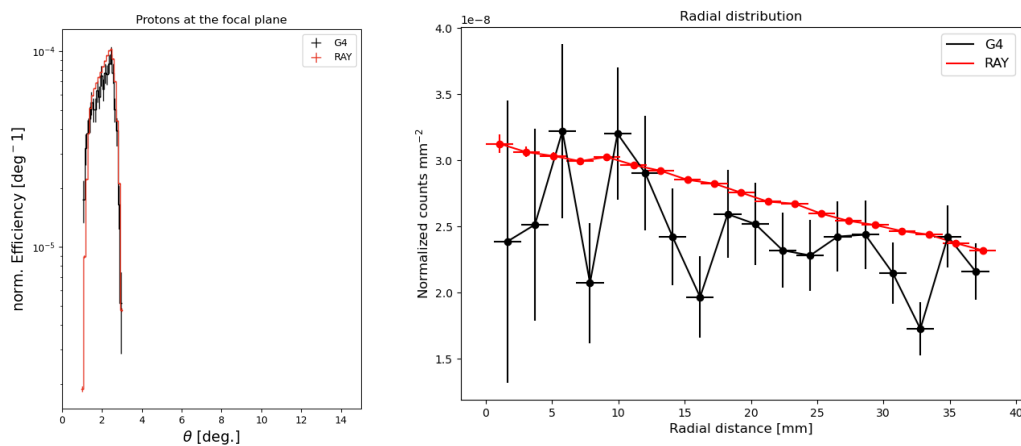

Figure 4: Comparison of the angular (left) and radial (right) distribution, after applying the factor 2 normalization in efficiency, between the Geant4 and ray-tracing simulation of the proton scattering at the XMM mirror for an input proton energy of 50 keV.

Two independent simulation frameworks, using different models for the physics interaction, provide similar angular and spatial distributions, but with a different normalization factor in the effective area, hence there is no need to build two simulation pipelines. While we consider this factor 2 discrepancy to provide the level of confidence to rely on when using the proton response files because of systematics in the proton scattering simulation accuracy, we selected the Geant4 simulation as the reference one to build the end-to-end simulation. The reasons are the followings:

- in the work of [12] both the elastic Remizovich and the Single Scattering models were compared against eROSITA scattering measurements and the Single Scattering predicted efficiency resulted closer to the laboratory data;
- the new Remizovich non-elastic approximation is an analytical expression obtained from modelling the laboratory experiment that covered a limited set of input energies and angles;

- in the Geant4 simulation, the Single Scattering uses theory-based cross-sections simulating every single collision[3] and the comparison against measurements was obtained using the physics list out-of-the-box without any adaptation.

1.4 Geant4 proton attenuation simulation (Task 1.4)

The focal plane assembly (FPA) surrounding the three EPIC cameras is the same. The main components of the Geant4 mass model of the EPIC FPA are, in addition to the cameras, the optical filters, the radiation shielding baffle, an Aluminum alloy baffle about 60 cm long placed at the top of the filter wheel, and surrounding structures modelled by a Titanium forward proton shield, 100 mm long (Fig. 5, left panel). While the presence of the radiation shielding is fundamental in reducing the non-focused particle-induced background (e.g., induced by galactic cosmic rays), in case of protons entering the field of view the secondary scattering at the baffle inner surface can potentially increase the background rate (see Sect. 5).

From top to bottom, we first encounter the Al proton shield (in grey) then the filter, the Ti forward proton shield (in yellow), and finally the camera at the focal plane. The figure also shows the entrance to the focal plane instruments (the door, in light green) and the filter wheel (in orange), which we did not simulate. We simply added a further Al truncated cone connecting the two proton shields, to simulate a closed environment and to avoid the dispersion of protons. The box surrounding the focal plane assembly is indicative to the reader and was not simulated.

The filter wheel is equipped with three different optical blocking filters [2] to reduce contamination from IR, visible and UV light collected in the field of view. With a diameter of 76 mm and placed at 10 cm from the focal plane, the observer can select among two thin filters, one medium filter and one thick filter (Table 2).

XMM-NEWTON OPTICAL FILTERS

Filter	Layer 1	Layer 2	Layer 3
thin	Al (0.04 μm)	Pl (0.16 μm)	
medium	Al (0.08 μm)	Pl (0.16 μm)	
thick	Tin (0.045 μm)	Al (0.11 μm)	PP (0.33 μm)

Table 2: The composition and thickness of the optical blocking filters. The layer numbering starts at the mirror side.

1.4.1 MOS focal plane assembly

The MOS camera is composed by 7 front-illuminated CCDs operating from 0.5 to 12 keV. Each CCD is divided into 600 × 600 pixels, each with an area of 40 × 40 μm. The central CCD is at the focal point on the optical axis of the telescope, while the others are at a distance of 4.5 mm towards the mirror, to approximately reproduce the focal plane curvature. Each CCD has a 300 μm-wide dead region on three sides. They are rotated and disposed in order to cover the dead sides as much as possible, to maximize the exposed area. An Aluminum ring, 100 μm thick, is placed on top the CCDs to represent the camera metalwork limiting the field of view to 62 mm of diameter. The Geant4 model of the MOS CCDs is shown in Figure 5, right panel.

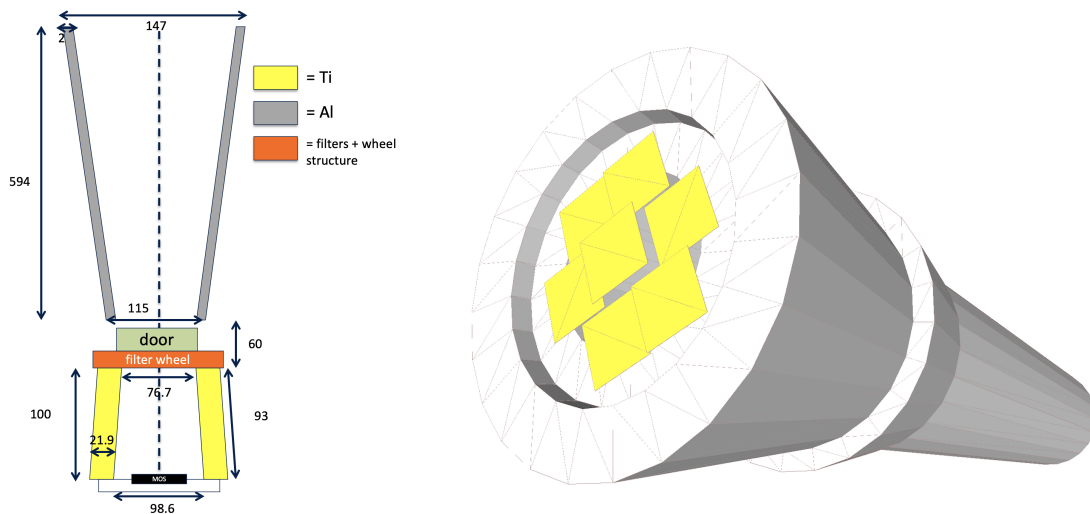[3] Geant4 Physics Reference Manual v10.4

Figure 5: Schematic view of the XMM-Newton focal plane assembly geometry (left) and the respective bottom view of the Geant4 mass model, with highlighted in yellow the MOS CCDs.

The MOS conventional 3-phase front-illumination device is characterised by an open electrode structure [20] where one of the electrodes was partially etched, i.e. holes were cut through it, to increase the X-ray detection efficiency at low energies. The resulting device structure [21, 22] is divided into a 60% portion covered by the standard closed electrode structure, composed by a layer of Si (0.3 μm thick) and SiO2 (0.75 μm thick), and a 40% area of open electrode with only 0.085 μm of SiO2. The depletion region, made of Silicon, is 37 μm thick. Fig. 6 (left panel) shows a not in scale schema of the pixel geometry implemented in Geant4. The X-ray detection efficiency generated by the MOS CCD pixels was measured on-ground by sampling different positions of the array [21]. The resulting mean pixel X-ray response is compared in Fig. 6 (right panel) to the Geant4 simulation of the MOS quantum efficiency obtained by illuminating the array with a uniform photon beam from 0.2 to 10 keV. The two curves are in very good agreement above 0.5 keV, with residuals within some percentage. Towards lower energies we find a degradation in the accuracy that reaches 20% at the low energy threshold. Since the work of [21] does not include uncertainties in the curve, it is difficult to explain the source of the discrepancy. However, the general agreement well within 20% positively verifies the Geant4 implementation of the MOS camera, a key factor in correctly estimating the proton energy losses.
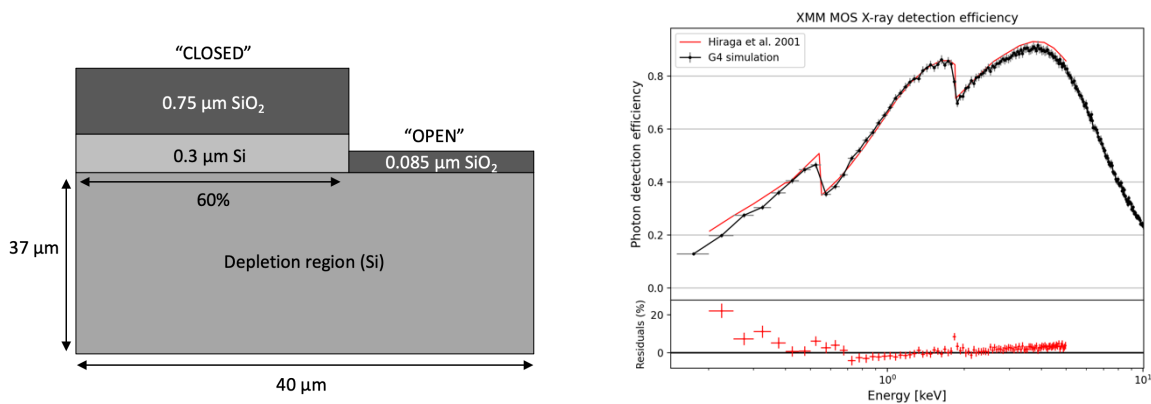

Figure 6: (left) Schematic side view, not in scale, of the MOS pixel geometry implemented in the simulation, with the open and closed electrode structure on top of the depletion region covering 60% and 40% of the pixel area respectively. (right) Comparison of the measured (red line) and simulated (black line) MOS X-ray detection efficiency (the error bars refer to the simulation statistical uncertainty).

The simulation of the proton transmission efficiency is obtained by randomly simulating protons within a circle with a diameter of 76 mm (equal to the filters), centered on the optical axis of the telescope and perpendicular to it. Proton energies are randomly generated in the range 2–300 keV, and then selected in the analysis in input bins of 1 keV to evaluate the transmission efficiency. The latter is defined as the number of protons that deposit energy within the MOS energy range over the total number of simulated protons within the bin. From the transmission efficiencies of all the simulated detectors we define a common input energy range of 2 - 300 keV. While the instrument proton detection efficiency is very low above 200 keV, we extended the upper limit to 300 keV to test the effect of secondary scattering with the baffle and surrounding volumes.

The MOS result is shown in Fig. 7, where two peaks in the transmission efficiency appear, one centered at ∼ 35 keV if protons cross the open electrode, and one centered at ∼ 160 keV if they encounter instead the thicker closed electrode. For the analytical computation, proton stopping powers reported by NIST[4] were used for all of the materials involved. The stopping power was interpolated using Mathematica[5], and the energy loss after each layer of the filters and the electrodes was calculated as a function of their thickness. As a result, we obtained the energy of the proton when impacting on the sensitive layer of the MOS detector, as a function of the incident energy and the thickness of each layer crossed by the particle, that were left as free controllable parameters in the computation to allow probing different configurations. The analytical computation defines an energy range where protons are able, according to the tabulated stopping power, to reach the MOS pixels without losing all their energy. Not only the two peaks predicted by the Geant4 simulations are confirmed by the tabulated stopping power, but the energy ranges are also consistent if we consider the uncertainties introduced by the angular spread and the complex geometry of the pixels.
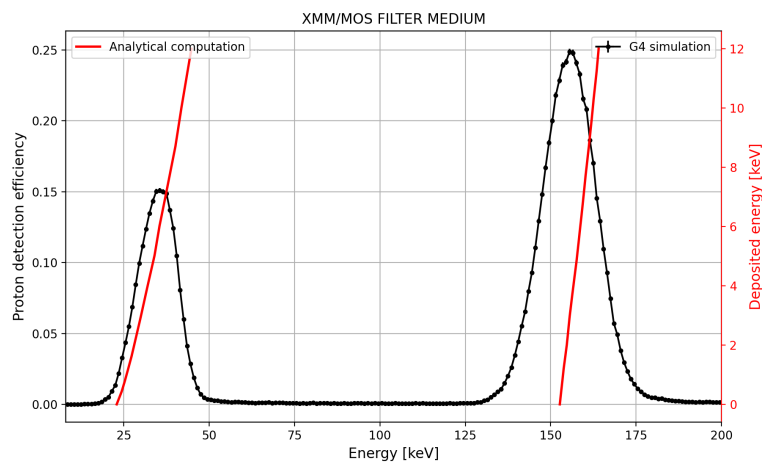

Figure 7: Simulated, in black, proton transmission efficiency in the 8 – 200 keV energy range for the MOS and medium filter. The analytical computation based on tabulated NIST proton stopping power predicts the proton energy range for which the MOS is likely to register a count, with an energy labelled by the red y-axis.

---

[4] https://physics.nist.gov/PhysRefData/Star/Text/PSTAR.html

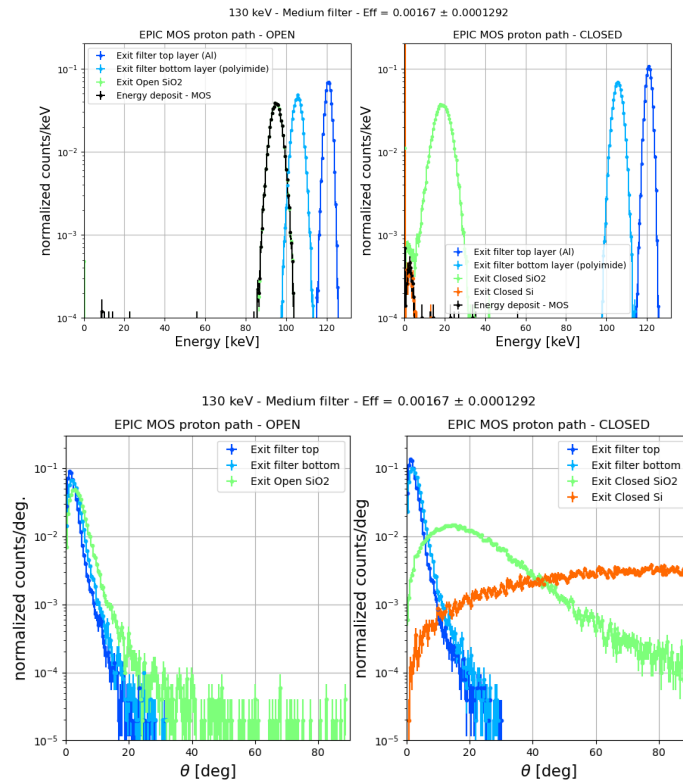[5] Wolfram Research, Inc., Mathematica, Version 9.0, Champaign, IL (2012)

Figure 8: Energy and angular distribution of the protons, for an input energy of 35 keV, exiting each layer of the medium filter and electrode structure, open in the left panel and closed in the right panel.

The proton energy and angular distribution at the exit of each layer was analyzed for a set of energies to verify the analysis pipeline processing the FPA simulation. Fig. 8 shows the result for a 35 keV input proton beam, where the transmission efficiency low energy peak is centered. About 20 keV are lost in the medium filter, and while the closed electrode absorbs the remaining energy, if protons reach the open structure their final energy falls in the 5–10 keV band. The proton direction spread, defined as the angle from the telescope axis, increases linearly while crossing the passive layers, and the medium filter alone introduces a $5° −$ $10°$ medium shift. This angular spread impacts the number of protons that are able to reach the detector, and the height of the filter from the focal plane is a parameter that can modify the soft proton-induced background. The front-illuminated device drastically increases the spread, and the protons lose the memory of their incident direction.

The successful verification of the Geant4 simulation of the EPIC optical filters and MOS electrode structure, by comparing both tabulated results and laboratory measurements, was a mandatory stepstone in the overall XMM end-to-end simulation. The resulting MOS detection efficiency for the three filters is shown in Fig. 9.
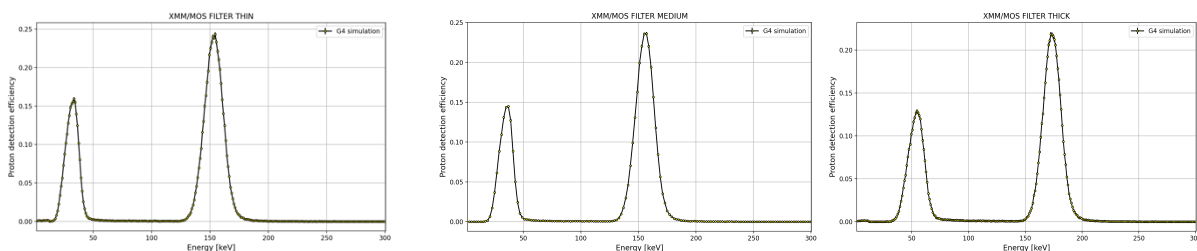

Figure 9: MOS FPA proton detection efficiency for a thin (left), medium (center) and thick (right) filter
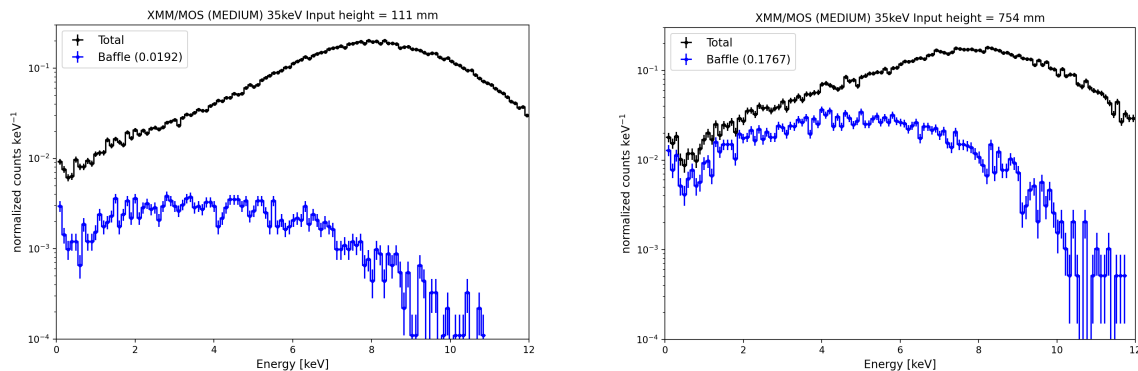
Figure 10: Soft proton induced X-ray spectra, for an incident energy of 35 keV, obtained extracting the mirror simulation proton list at a height of 111 mm (at the optical filter, left panel) and 754 mm (the baffle entrance, right panel). Protons interacting with the baffle surface before generating a count on the MOS are highlighted in blue, and their fraction concerning the total is reported in the legend.

The impact of the proton shield in scattering soft protons was tested with the MOS camera as a use case, by extracting the output of the mirror simulation at two heights: 754 mm, the baffle entrance, and 111 mm, at the optical filter. Using the baffle flag of data level 1 (Sect. 3.1), we can estimate the fraction of protons that scatter with the focal plane baffle before generating the background event. The result is shown in Fig. 10. The fraction of protons that scatter with the radiation shielding increases from 2% for a height of 111 mm (left) to $\sim$ 18% for the 754 mm case (right). Protons scattering with the baffle surface lose energy and increase the low energy tail of the spectrum. This effect is visible in the plot, softening the background spectral distribution.

For this reason, in the XMM FPA simulation protons were generated at the top of the baffle. We note, however that when taking into account the whole input energy range and considering the general uncertainties of the simulation set-up, the final background flux generated by two prototypes of the proton response files, obtained at 754 and 111 mm input protons, the impact of the baffle is no longer visible (Fig. 11). The statistical uncertainties are instead much more improved if protons are generated at the optical filters. For this reason, in the WFI FPA simulation (see Sect. 2.4) the protons were simulated at the filter wheel height, i.e. we have chosen to increase the statistics while neglecting the impact of secondary scattering.
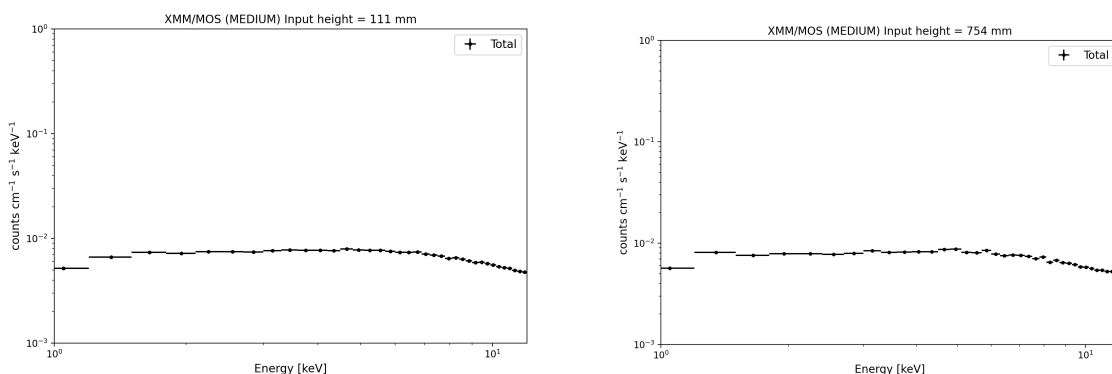

Figure 11: Soft proton induced background flux obtained simulating protons at the optical filter (left) and baffle entrance (right).

In the Geant4 FPA simulation, the output of the mirror simulation is used as input (see Sect. 3.2 for details) and the energy deposits in the depleted region of the pixels are stored in output files, with their position and

an associated flag if the proton interacts with the baffle. The raw simulation output is then reconstructed into a list of counts, where all the energy deposits within the same pixel in the same event are summed up. A count is a total energy deposit within the MOS energy range (0.2 - 12 keV). Fig. 12 (left) shows the count map produced by a 35 keV proton entering the mirror.
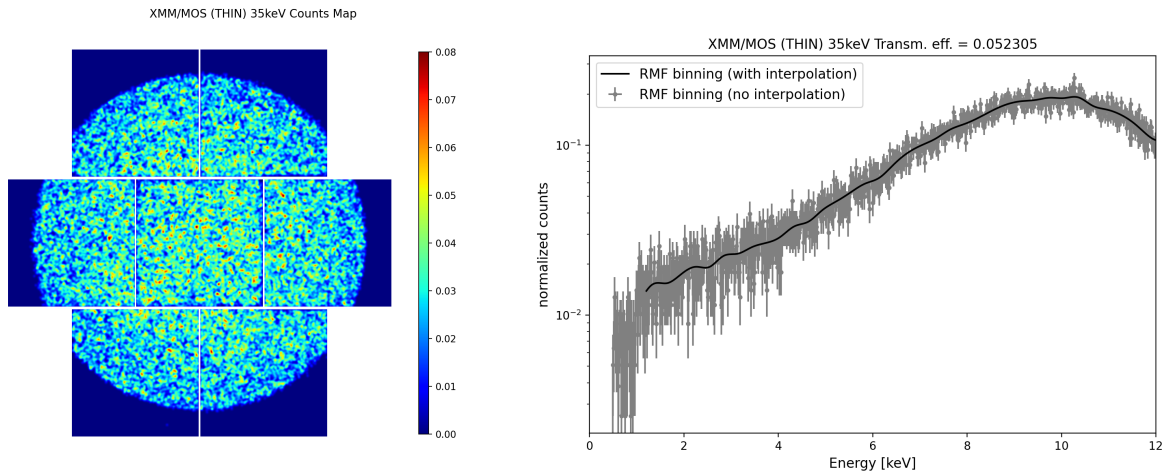

Figure 12: MOS (medium filter) counts map (left) and interpolation of the spectral distribution (right) for an input energy of 35 keV at the mirror entrance.

The counts are first binned using the X-ray RMF channels (see Sect. 3.1), as shown in grey in Fig. 12 (right). Statistical errors dominate the plot, and the energy distribution cannot be directly stored in the proton RMF.

The adopted solution was to rebin and interpolate the histogram, the black curve of Fig 12 (right), and use the interpolation function to fill the RMF. If the number of counts was not enough to produce a histogram in the first place, a constant was used along the covered energy range. This method allowed to automatically generate the RMF model for all the input energies despite the limited statistics, but it also caused some caveats in the proton response file usage. The interpolation function produces artefacts at the border of the energy range, in particular when the count number is low. We tested (see Sect. 3.3) each response matrix against a standard simulation - where no artefacts are present since there is no interpolation - and defined a validity energy range for the use of the response files from this comparison.

We also note the cut in the MOS energy spectrum at about 1 keV (Fig. 12, right). Since the accuracy of the Geant4 modelling of the proton stopping power degrades below 1 keV (20% at 1 keV reported in the Geant4 Physics Reference Manual[6]), the simulated proton efficiency at the detector also features a reduction at low energy that is not physical but caused by internal limits in the Geant4 physics model. For this reason, the energy redistribution is modelled from 1 keV to the upper threshold of the instrument X-ray RMF.

1.4.2 PN focal plane assembly

The PN camera [2] is instead back-illuminated, composed of four quadrants each having three CCDs with 200×64 pixels, with a pixel size of 150×150 μm and a total imaging area of 6×6 cm. The fully depleted Silicon thickness is 300 μm. Being back-illuminated, no read-out devices are present in front of the PN

---

[6] https://geant4-userdoc.web.cern.ch/UsersGuides/PhysicsReferenceManual/BackupVersions/V10.4/html/index.html

camera, simplifying its Geant4 implementation. In addition, no metalwork is placed on top of the camera and contrary to the MOS, all the CCD area is exposed to the soft proton flux.

The PN proton transmission efficiency for the three filters is shown in Fig. 13. We note that with the lack of the electrode multi-structure on top, there is only one peak in the efficiency.
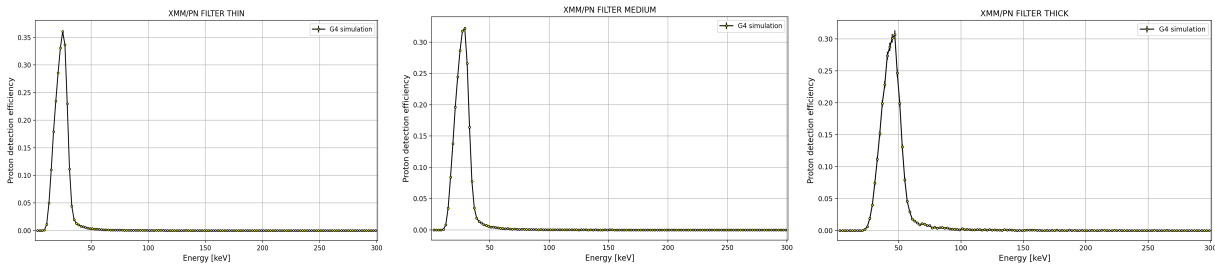

Figure 13: PN FPA proton detection efficiency for a thin (left), medium (center) and thick (right) filter.

The PN counts map, in the 0.2 - 20 keV energy range, is shown in Fig 14 (left) for an input proton energy of 35 keV. The RMF for the PN followed the same method of the MOS, with the energy spectrum first re-binned and interpolated, and then the interpolation function was used to fill the same channels of the X-ray RMF (Fig. 14, right).
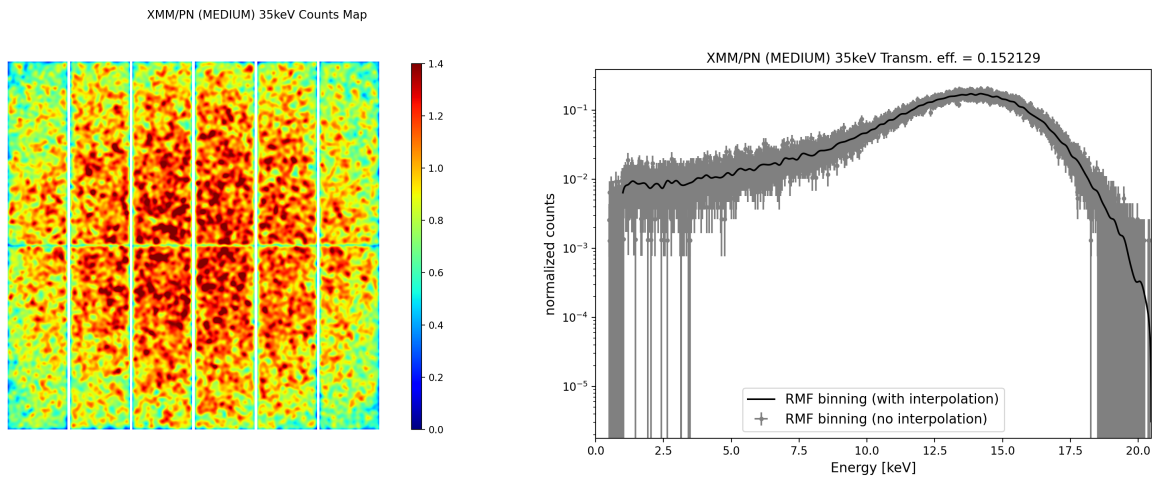

Figure 14: PN (medium filter) counts map (left) and interpolation of the spectral distribution (right) for an input energy of 35 keV at the mirror entrance.